Theory of Offset-Continuation Trajectory Stack

Tiago A. Coimbra*, Amélia Novais and Jörg Schleicher, University of Campinas / INCT-GP

Abstract

We employ the term offset-continuation trajectory stack, or briefly OCT stack, to describe the act of computing efficiently the data stack along approximate common-reflection-point (CRP) trajectories. The method allows to construct a stacked common-offset gather, that may have (or not) been collected in the field. In other words, it is a data-driven stacking technique that transforms 2D/2.5D prestack multicoverage data into a common-offset (CO) section. Similarly to the CMP and CRS stacks, this new method does not rely on an a-priori velocity model but provides velocity information itself. The original offset-continuation-operation (OCO) method is a seismic configuration transform designed to simulate a seismic section as if obtained with a certain source-receiver offset using the data measured with another offset. Since an OCO depends on the velocity model used in the process, it can be combined with stacking techniques for a set of models, thus allowing for the extraction of velocity information. The algorithm is based on so-called OCO trajectories, which are related to the concepts of image waves and velocity rays. We theoretically derive the OCO trajectories from the kinematic properties of OCO image waves that describe the continuous transformation of the common-offset reflection event from one offset to another. Based on OCO trajectories, we then formulate a horizon-based velocity-analysis method, where root mean square (RMS) velocities and local event slopes are determined by stacking along event horizons. A numerical example demonstrates the feasibility of the method.

Introduction

For data of very low signal-to-noise (S/N) ratio or acquisitions with very low fold, conventional common-midpoint (CMP) processing might not provide stacked sections of sufficient quality. In such situations, alternative processing sequences making use of a higher fold are necessary to improve the data quality. Common-reflection-surface stack (see, e.g., Höcht et al., 1999; Jäger et al., 2001; Hertweck et al., 2007) and multifocusing (Gelchinsky et al., 1999) are such generalized stacking techniques. Here we propose an alternative technique that also makes use of a higher data fold. We refer to this new process, which is based on the offset-continuation operation (OCO), as offset-continuation trajectory stack or briefly OCT stack. It represents such an alternative path for the processing of reflection-seismic data. Its key element is the construction of common-offset stacked sections together with coherency sections and sections of kinematic and dynamic wavefield attributes.

By definition, the Offset-Continuation Operation (OCO) is an operator that transforms common offset (CO) seismic gathers from one constant offset to another (Deregowski and Rocca, 1981). It is an important tool for imaging in a complex medium. Possible applications of OCO include velocity analysis, common-reflection point (CRP) stacking, dip moveout (DMO), migration to zero offset (MZO), interpolation of missing data, amplitude variation with offset (AVO) studies, and geometrical-spreading correction (see, e.g., Salvador and Savelli, 1982; Bolondi et al., 1982, 1984; Fomel, 1994, 2003; Santos et al., 1997).

Since OCO is a configuration transform, its objective is to simulate a seismic section using as input the data measured with another configuration. As discussed by Hubral et al. (1996a) and mathematically demonstrated by Tygel et al. (1996), any configuration transform can be thought of as being composed of a migration and a subsequent demigration after changing a configuration parameter.

Configurations transforms have already been used for several purposes in seismic processing such as MZO (Tygel et al., 1998; Bleistein et al., 1999), source continuation operation (SCO) (Bagaini and Spagnolini, 1993, 1996), azimuth moveout (AMO) (Biondi et al., 1998), DMO (Hale, 1984; Canning and Gardner, 1996; Collins, 1997; Black et al., 1993), common-source (CS)-DMO (Schleicher and Bagaini, 2004), data reconstruction (Bagaini et al., 1994; Stolt, 2002; Chemingui and Biondi, 2002), and velocity analysis (Silva, 2005; Coimbra et al., 2012).

The OCT stack makes use of so-called OCO trajectories (Coimbra et al., 2012). Such a trajectory requires only two parameters (local event slope and stacking velocity) to describe the seismic reflection event in the multi-coverage data. Using these parameters, the method stacks the data along a predicted traveltime curve that approximates the CRP event. Since the parameters, and thus the predicted traveltime curve, are updated from the data at each offset, the approximation is better than by conventional methods that adjust the approximate traveltime expression at some initial point. The purpose of this paper is to establish a consistent processing chain that is based entirely on the OCT stack, relying on identical assumptions at all steps.

Theoretical description

Coimbra et al. (2013) derived the theoretical basis for the stack along OCO trajectories, based on the kinematic

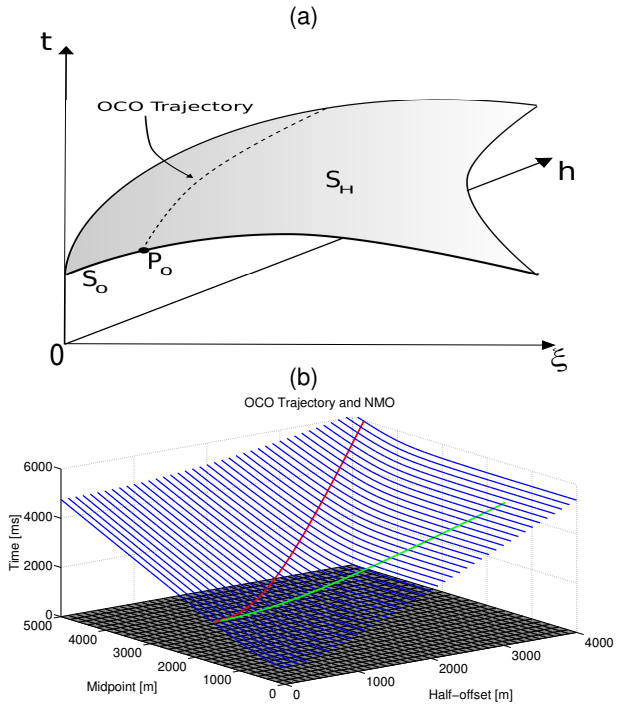

Figure 1: *Sketch representing a traveltime surface and an OCO trajectory starting at a point P_0 on the traveltime curve S_0 in the initial common-offset section with half-offset h_0 (front panel). (b) Location of an OCO trajectory (red line) as compared to CMP traveltime curves (green line).*

behaviour of the OCO transformation as described by the OCO image-wave equation (Hubral et al., 1996b). Here we briefly summarize the main theoretical ideas.

OCO trajectories

Recently, Coimbra et al. (2012) derived the OCO trajectory tracing system has been recently derived by means of applying the method of characteristics to the second-order linear partial differential equation known as the OCO image-wave equation (Hubral et al., 1996b). Formally, we can think of the solution to this equation as being approximated by an expression that is analogous to the one used in ray theory, i.e., the leading term of a high-frequency asymptotic (WKBJ-type) approximation for a reflected wave recorded on a seismogram. Thus, the leading high-frequency term describes the image-wave front for the OCO image wave. In other words, the image-wave front can be thought of as being represented by an OCO eikonal, governed by an image-eikonal equation.

The solution of the OCO eikonal equation leads to ray-like trajectories describing the position of a selected point P_0 on a seismic reflection event S_0 in different common-offset sections, the so-called OCO trajectories (Coimbra et al., 2012, see also Figure 1a). In other words, an OCO trajectory is the curve described by one event point under variation of offset.

The algebraic procedure to construct the OCO trajectories can be summarized as follows. As shown by Coimbra et al. (2013), the traveltime surface in the offset-midpoint-time space is a manifold $S_H(t,\xi,H)=0$ (see again Figure 1a), where H is the OCO eikonal. It must satisfy

$$H(\xi_h, t_h(\xi_h)) = h, \tag{1}$$

in all common-offset sections. At $h=h_0$, the manifold S_H coincides with the reflection event

$$S_0 = S_H(t(h_0,\xi_{h_0}),\xi(h_0,\xi_{h_0}),h_0) = 0\ . \tag{2}$$

This leads to a family of characteristic curves $t=t(h,\xi_{h_0})$, $\xi=\xi(h,\xi_{h_0})$, and $H=H(h,\xi_{h_0})$, which depend on ξ_{h_0} and h as parameters. Fixing $h=h_0$ and varying ξ_{h_0} we obtain the curve S_0. On the other hand, fixing ξ_{h_0} and varying h, we obtain the OCO trajectories. Actually, Santos et al. (1997) have demonstrated that for one fixed ξ_{h_0}, all possible OCO trajectories must satisfy

$$t^2 = t(\xi,h;\xi_{h_0},t_{h_0},h_0)^2 = \frac{4h^2}{V^2} + \frac{4h^2(t_{h_0}^2 - 4h_0^2/V^2)}{u^2}\ , \tag{3}$$

with

$$u = \sqrt{(h+h_0)^2-(\xi-\xi_{h_0})^2} + \sqrt{(h-h_0)^2-(\xi-\xi_{h_0})^2}\ .$$

Equation (3) is also known as the OCO Huygens-image curve. It depends on the parameters ξ, h, ξ_{h_0}, t_{h_0} and h_0, but is independent of the actual position of the event through P_0.

The actual path of the OCO trajectory depends on the event slope at P_0. To describe this dependence, we parameterize $t_{h_0}=t_{h_0}(\xi_{h_0})$ and consider ξ_{h_0} as a function of ξ, h and h_0. The envelope of all OCO Huygens image-curves for all points on S_0 describes the manifold S_H at half-offset h. It is constructed by taking the derivative of t in equation (3) with respect to ξ_{h_0}. This results in the relationship between the position ξ of the event at half-offset h to its position ξ_{h_0} at h_0 given by

$$\xi = \xi(h;\xi_{h_0},t_{h_0},\phi_{h_0},h_0) = \xi_{h_0} + 2\Upsilon_{h_0}(h^2-h_0^2)/Q\ , \tag{4}$$

where $Q = \sqrt{\Upsilon_{h_0}^2\eta^2 + 2t_{n_0}^4 + 2\sqrt{t_{n_0}^8 + \Upsilon_{h_0}^2 t_{n_0}^4\eta^2 + 16\Upsilon_{h_0}^4 h^2 h_0^2}}$. Here, $t_{n_0}=\sqrt{t_{h_0}^2 - 4h_0^2/V^2}$ is the NMO corrected traveltime at the initial half-offset h_0, $\eta = 2\sqrt{h^2+h_0^2}$, and $\Upsilon_{h_0}=t_{h_0}\phi_{h_0}$, with ϕ_{h_0} denoting the dip of the reflection event S_0 at P_0.

Together, equations (3) and (4) constitute a parametric form of the manifold S_H. For a fixed ξ_{h_0} these equations thus describe the OCO trajectory from P_0 to any other common-offset at h. In other words, equations (3) and (4) represent the position of events that are reflected at the same point in depth (if the medium was exactly described by the OCO velocity V), i.e., the OCO trajectory belongs to a common-reflection point (CRP).

The OCO trajectory starting at some initial half-offset $h_0 = h_i \neq 0$ and ending at the final half-offset $h=0$ can be alternatively described in the opposite direction as starting as $h_0=0$ and ending at h_i. Thus, their midpoint dislocations $\xi_0-\xi$ must be the same. This leads to the relationship between the event slopes in the CO(h_0) and CO(h) sections given by

$$\phi_h = \phi_{h_0}\left(t_n^2 t_{h_0} \Big/ t_{n_0}^2 t\right)\ , \tag{5}$$

where $t_n=\sqrt{t^2-4h^2/V^2}$ is the NMO corrected traveltime at half-offset h.

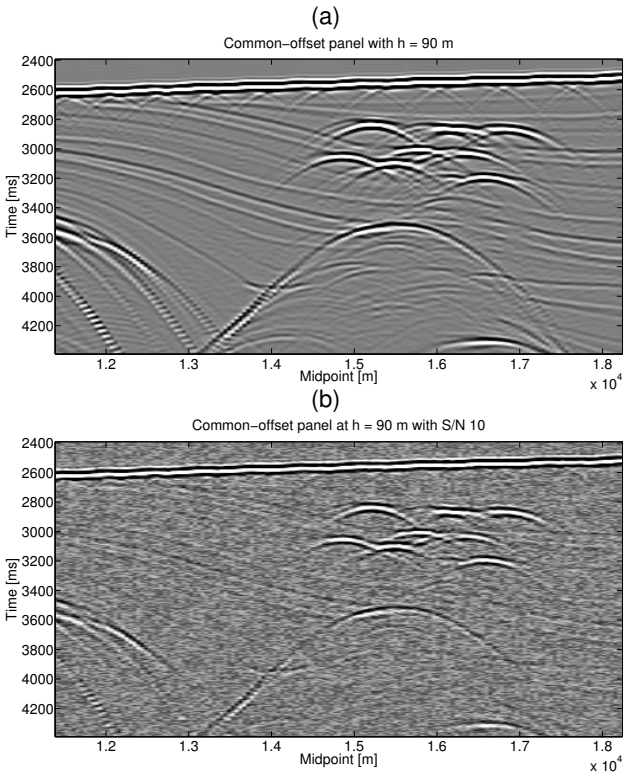

Figure 2: *(a) CO section at $h = 90m$ for synthetic test of stacking along OCO trajectories, (b) Noisy reference CO section (S/N=10).*

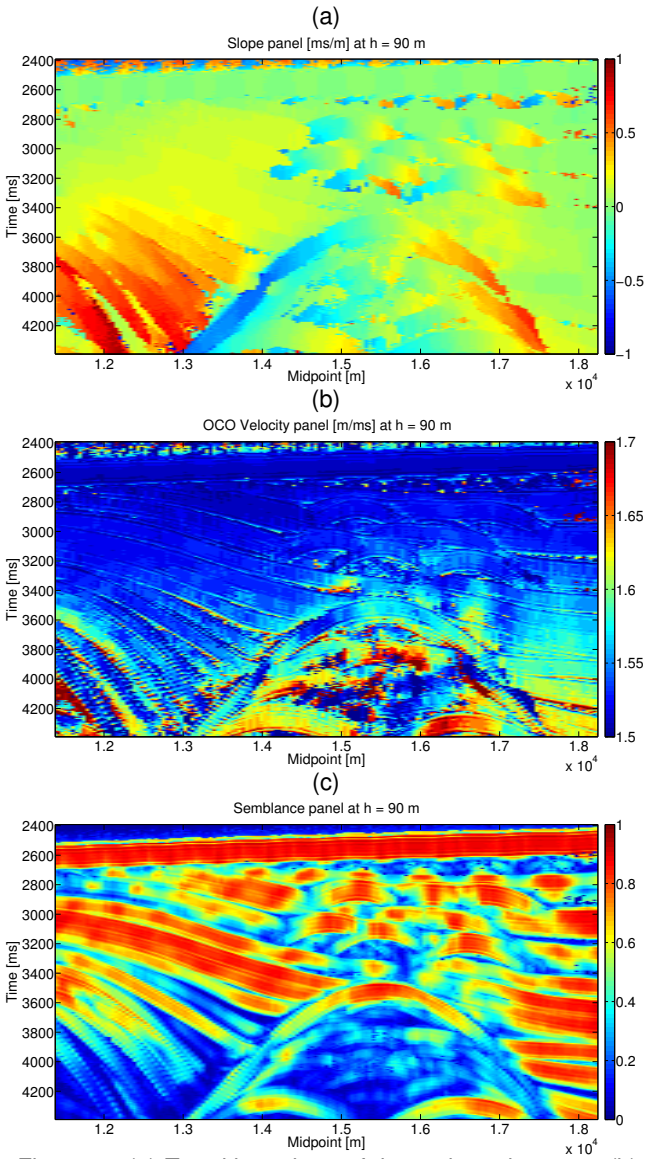

Figure 3: *(a) Traveltime slope of the major coherence, (b) OCO velocity panel. (c) Semblance along OCO trajectory of the major coherence.*

Stack along OCO trajectories

The OCO trajectories can be used to approximate the traveltime surface using the set of equations (3), (4), and (5). Along the best-fitting trajectories, the data can be stacked in a similar manner to conventional stacking techniques. The best-fitting OCO trajectories are found as follows: For a central point P_0 with coordinates $(\xi_{h_0}, t_{h_0}, h_0)$, we trace trial OCO trajectories for each possible combination of values for V and ϕ_{h_0}. The pair that provides a coherence along the trial trajectory defines the OCO trajectory for P_0. To incorporate information about the time dip along the trial trajectories, the coherence is evaluated along the dip direction in a small window of neighboring traces (7 traces in our implementation) around the trajectory. At each half-offset, the dip is corrected from its initial value by means of equation (5).

Denoting the parameter pair of local event dip ϕ_{h_0} and average velocity V for the so-determined best-fitting OCO trajectory as $\Xi = (\phi_{h_0}, V)$ to simplify the notation, the OCT stack can be written as

$$M(P_0;\Xi,h) = \int_{h_0}^{h} \sum_{n=-N}^{N} U(\xi(\gamma,\xi_n;\Xi), t(\gamma,\xi_n;\Xi), \gamma) d\gamma \,, \qquad (6)$$

where $\xi_n = \xi_{h_0} + n\Delta\xi$ is the location of the nth neighboring trace in the initial CO section, $U = U(\xi,t,h)$ is reflection seismic data in the midpoint-time-offset domain and N (3 in our implementation) is number of traces to each side of the principal trace that define the dip window.

The stacking procedure can be modified to improve the treatment of conflicting dips. For this purpose, we calculate the coherence-weighted average over all stacking results for different dips obtained with the same mean velocity V that provided the best-fitting OCO trajectories. In symbols,

$$M_s(P_0) = \langle M(P_0,\Xi)\rangle_V = \frac{\int_{\phi_1}^{\phi_2} C_M(P_0,\Xi) M(P_0;\Xi,h) d\phi_{h_0}}{\int_{\phi_1}^{\phi_2} C_M(P_0,\Xi) d\phi_{h_0}} \,, \qquad (7)$$

where C_M is coherence measured in this case was used a variation of the Semblance (Neidell and Taner, 1971).

Traveltime derivatives

There are a number of useful relationships between different types of traveltime derivatives that can be found from the set of equations (1)-(4). On the traveltime curve in the common-offset section at h, we can differentiate equation (1) with respect to ξ and h provide two important relationships between the local event slopes in the CO section, ϕ_h, and in the CMP section, ψ_ξ, at the point (ξ,h)

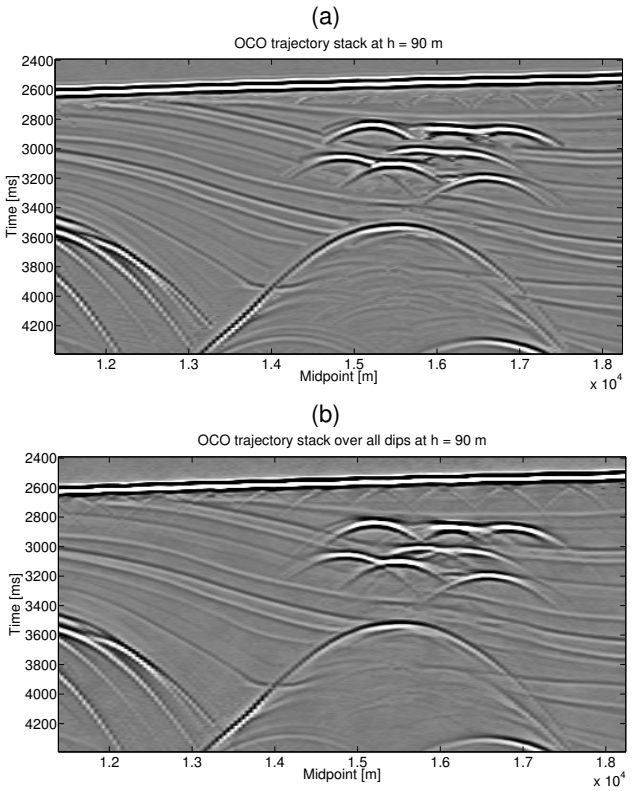

Figure 4: *(a) Initial OCT stacked section. (b) Final OCT stacked section with improved treatment of conflicting dips.*

where these sections intersect. The fact that the total derivative of H with respect to ξ on the event is identically zero, leads to (Coimbra et al., 2012)

$$\phi_h = \left.\frac{\partial t}{\partial \xi}\right|_h = -\frac{\partial H}{\partial \xi}\left(\frac{\partial H}{\partial t}\right)^{-1} , \qquad (8)$$

which relates the traveltime slope ϕ in the CO section. Correspondingly, from $dH/dh = 1$, we find that the traveltime slope ψ in the CMP section as

$$\psi_\xi = \left.\frac{\partial t}{\partial h}\right|_\xi = \frac{dH/dh}{\partial H/\partial t} . \qquad (9)$$

Hubral et al. (1996b) found another useful equation for the midpoint displacement in terms of the derivatives of H. In our notation, their equation (A29) can be written as

$$\xi_h - \xi_0 = \frac{\phi_h h^2}{t - h\psi_\xi} . \qquad (10)$$

By substituting equation (4) with $h_0 = 0$ into formula (10), we find after some tedious manipulations an expression for the local event slope ψ_ξ in the CMP section at ξ as a function of the local event slope ϕ_h in the CO section at h. It reads

$$\psi_\xi = \frac{2ht(4-\phi_h^2V^2)}{V^2t^2+4h^2+\sqrt{16h^4-4h^2t^2V^2(\phi_h^2V^2+2)+t^4V^4}} . \qquad (11)$$

It is instructive to observe that for a horizontal event, i.e., in the case of $\phi_h = 0$, equation (11) simplifies considerably to

$$\psi_\xi = \frac{4h}{V^2t} . \qquad (12)$$

Using that $\xi = (s+g)/2$ and $h = (g-s)/2$, where s and g are the source and receiver coordinates, we also find the traveltime derivatives with respect to s and g, i.e., the event slopes at the corresponding points in the respective common-shot and common-receiver sections, as

$$\varphi_s = \frac{\partial t}{\partial s} = \frac{1}{2}\left(\frac{\partial t}{\partial \xi} - \frac{\partial t}{\partial h}\right) = \frac{\phi_\xi - \psi_h}{2} , \qquad (13)$$

$$\varphi_g = \frac{\partial t}{\partial g} = \frac{1}{2}\left(\frac{\partial t}{\partial \xi} + \frac{\partial t}{\partial h}\right) = \frac{\phi_\xi + \psi_h}{2} . \qquad (14)$$

OCO velocity and RMS velocity

Let us now briefly discuss the relationship between the OCO and RMS velocities. For the case of $h_0 = 0$ in a homogeneous medium, differentiation of equation (11) with respect to h yields

$$\frac{\partial^2 t}{\partial h^2} = \frac{\partial \psi_\xi}{\partial h} = 2t(4-\phi_h^2V^2)/\Lambda + \mathscr{O}(h) , \qquad (15)$$

with $\Lambda = V^2t^2 + 4h^2 + \sqrt{16h^4 - 4h^2t^2V^2(\phi_h^2V^2+2)+t^4V^4}$. The second traveltime derivative in the CMP section at $h = 0$ is closely related to the NMO velocity v_n, because v_n defines the hyperbolic traveltime approximation $t^2 = t_0^2 + 4h^2/v_n^2$. Thus, expression (15) taken at $h = 0$ and multiplied by t_0 yields

$$t_0 \left.\frac{\partial^2 t}{\partial h^2}\right|_{h=0} \equiv \frac{4}{v_n^2} = \frac{4}{V^2} - \phi_0^2 . \qquad (16)$$

In other words, the OCO average velocity V is related to the NMO velocity v_n as

$$\frac{4}{V^2} = \frac{4}{v_n^2} + \phi_0^2 . \qquad (17)$$

While this expression may be hard to interpret in the general case, it is instructive to note that for a stack of dipping layers with dip angle β_M, $v_n = v_{rms}/\cos\beta_M$ and $\phi_0 = 2\sin\beta_M/v_{rms}$, which yields

$$V = v_{rms} . \qquad (18)$$

Note that this identity between the OCO velocity V and the RMS velocity v_{rms} is true at the very beginning of the OCO trajectory at zero offset. For OCO trajectories traced from another initial offset, V will deviate from the RMS velocity. In other words, an OCT stack allows to extract offset-depending average velocities.

Numerical results

To test the OCT stacking technique as described above, we have applied it to a synthetic multi-coverage data set, being a noise-contaminated subset of the Sigsbee2B data. Figure 2a shows a common-offset section for $h = 90$ m of the used part of the original Sigsbee2B data, and Figure 2b shows the corresponding noisy section with random noise with a S/N ratio of 10.

Figures 3-5 illustrate the procedure. For each point in the reference CO section for $h = 90$ m (Figure 2a), we applied the OCT stack to the noisy multi-coverage data. The maximum semblance (Figure 3c) along all trial OCO trajectory determines the parameter pair of traveltime slope

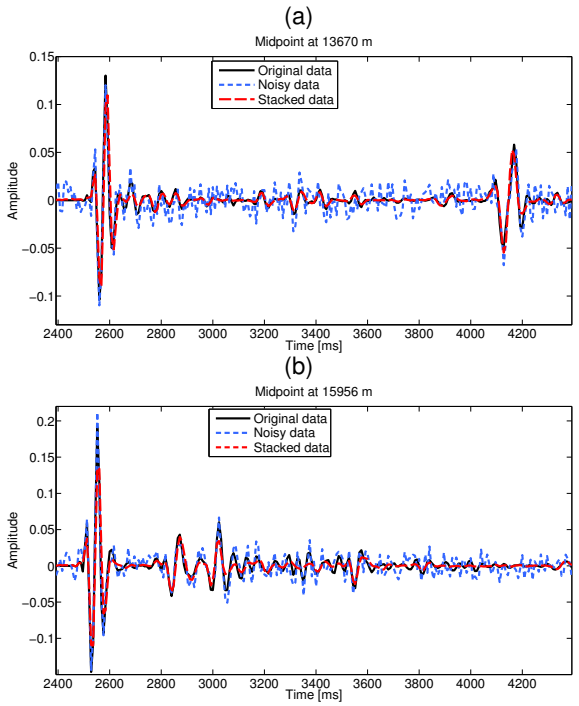

Figure 5: *Comparison between original (black, solid), noisy (blue, short dashes), and stacked (red, long dashes) traces. (a) $\xi_{h_0} = 13.670$ km, (b) $\xi_{h_0} = 15.956$ km.*

(Figure 3a) and OCO velocity (Figure 3b) that define the best-fitting OCO trajectory through the multi-coverage data.

The result of the stack using these values, equation 6, is a noise-attenuated stacked CO section (Figure 4a) corresponding to the reference section (which can, but need not exist among the acquired data). We observe a strong noise reduction in comparison to the noisy data section in Figure 2b. All strong events are nicely recovered. However, at points of conflicting dips, weaker events are suppressed.

The coherence-weighted average of all stacking results for all possible event slopes, equation 7, improves the treatment of conflicting dips (see Figure 4b). Particularly the diffraction events in the upper part of the section, but also other events with conflicting dips, are strongly improved. A drawback of the coherence weight is that weaker events are further reduced.

Figure 5 shows a trace-to-trace comparison of the original noise-free Sigsbee2B data, the corresponding noisy data, and the OCT stacked section at two positions with and without strong diffraction events. We see that the stacked traces recover the original traces almost perfectly, with a slight amplitude loss of some events.

Finally, an amplitude variation with offset (AVO) analysis becomes possible along a very good approximation to the true CRP trajectory. Figure 6 compares a conventional CMP section with a CRP section obtained by selecting data along OCO trajectories. Within both circles in Figure 6 we see that there exist a significant difference between amplitudes of both data along certain events, indicating that an AVO analysis in the CRP section would provide improved results over those from the CMP section.

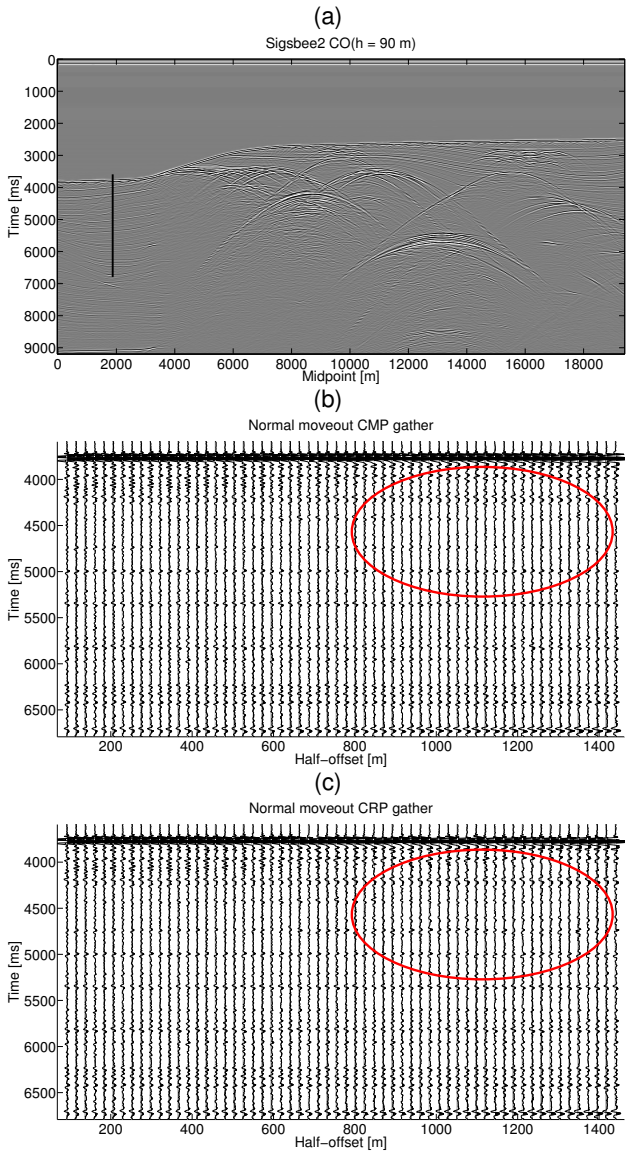

Figure 6: *(a) Sigsbee2B data near-offset section, (b) Normal moveout CMP panel. (c) Normal moveout CRP panel.*

Discussion

OCO trajectories (Coimbra et al., 2012) can be used for a multiparameter stacking procedure similar to its relatives, the CMP and CRS stacks and multifocusing. By stacking along trial trajectories, the OCO trajectory (OCT) stack automatically determines stacking attributes based on a coherence measure applied at every common-offset sample of the data. The main advantages of the OCO trajectories are twofold. Firstly, in comparison to a CMP or zero-offset CRS stack, the procedure is not limited to a zero-offset stacked section. This allows for the construction of stacked common-offset sections to improve the signal-to-noise ratio or even to interpolate the data. Secondly, in comparison to an offset CRS stack, the OCO trajectory stack needs less parameters to construct the stacked CO sections. In the 2D/2.5D case as discussed here, only two parameters (stacking velocity and local traveltime slope) are needed.

Conclusions

We have developed a new method for stacking data into zero or common-offset sections. The method uses the tracing of offset continuation (OCO) trajectories. These trajectories describe the position of a selected point on a seismic reflection event as a function of offset. Neighbouring OCO trajectories form a stacking surface along which the data can be summed up. In this way, stacked common-offset sections can be constructed for any arbitrary offset. An OCO trajectory is described by only two parameters, being an average velocity that is an approximation to RMS velocity, and the local event slope in the final stacked section. This procedure is advantageous over an offset CRS stack, which needs at least 5 parameters to describe the stacking surface. As a byproduct, the stacking along OCO trajectories provides local event slopes at all offsets of interest, which can be of further use in tomographic methods.

Acknowledgements

This work was kindly supported by the Brazilian agencies CAPES, FINEP, and CNPq, as well as Petrobras and the sponsors of the *Wave Inversion Technology (WIT) Consortium*. We specially thank the SMAART-JV for providing the Sigsbee2B_nfs data and model.

References

Bagaini, C., and U. Spagnolini, 1993, Common-shot velocity analisys by shot continuation operators: 63rd Annual International Meeting., SEG, Expanded Abstracts., 673–676.

———, 1996, 2D continuation operators and their applications: Geophysics, **61**, 1846–1858.

Bagaini, C., U. Spagnolini, and V. Pazienza, 1994, Velocity analisys and missing offset restoration by prestack continuation operators: 64th Annual International Meeting., SEG, Expanded Abstracts., 673–676.

Biondi, B., S. Fomel, and N. Chemingui, 1998, Azimuth moveout for 3-D prestack imaging: Geophysics, **63**, 574–588.

Black, J., K. Schleicher, and L. Zhang, 1993, True-amplitude imaging and dip moveout: Geophysics, **58**, 47–66.

Bleistein, N., J. Cohen, and H. Jaramillo, 1999, True-amplitude transformation to zero offset of data from curved reflectors: Geophysics, **64**, 112–129.

Bolondi, G., E. Loinger, and F. Rocca, 1982, Offset continuation of seismic sections: Geophysical Prospecting, **30**, 813–828.

———, 1984, Offset continuation in theory and pratice: Geophysical Prospecting, **32**, 1045–1073.

Canning, A., and G. H. F. Gardner, 1996, Regularizing 3D data sets with DMO: Geophysics, **61**, 1101–1114.

Chemingui, N., and B. Biondi, 2002, Seismic data recostruction by inversion to common offset: Geophysics, **67**, 1575–1585.

Coimbra, T. A., A. Novais, and J. Schleicher, 2012, Offset continuation (OCO) ray tracing using OCO trajectories: Stud. Geophys. Geod., **56**, 65–82.

———, 2013, Stacking on OCO trajectories: Presented at the 75th Conference & Exhibition, EAGE.

Collins, C. L., 1997, Imaging in 3D DMO; Part I: Geometrical optics model; Part II: Amplitude effects: Geophysics, **62**, 211–244.

Deregowski, S. M., and F. Rocca, 1981, Geometrical optics and wave theory of constant offset sections in layered media: Geophysical Prospecting, **29**, 374–406.

Fomel, S., 1994, Kinematically equivalent differential operator for offset continuation of reflected wave seismograms: Russian Geology and Geophysics, **35**, 122–134.

———, 2003, Theory of differential offset continuation: Geophysics, **68**, 718–732.

Gelchinsky, B., A. Berkovitch, and S. Keydar, 1999, Multifocusing homeomorphic imaging - Part 1. Basic concepts and formulas: Journal of Applied Geophysics, **75**, 229–242.

Hale, I. D., 1984, Dip-moveout by fourier transform: Geophysics, **49**, 741–757.

Hertweck, T., J. Schleicher, and J. Mann, 2007, Data stacking beyond CMP: The Leading Edge, **26**, 818–827.

Höcht, G., E. de Bazelaire, P. Majer, and P. Hubral, 1999, Seismics and optics: hyperbolae and curvatures: J. Appl. Geoph., **42**, 261–281. (Special Issue on "Macro-Model Independent Seismic Reflection Imaging").

Hubral, P., J. Schleicher, and M. Tygel, 1996a, A unified approach to 3-D seismic reflection imaging - Part I:Basic concepts: Geophysics, **61**, 742–758.

Hubral, P., M. Tygel, and J. Schleicher, 1996b, Seismic image waves: Geoph. J. Int., **125**, 431–442.

Jäger, R., J. Mann, G. Höcht, and P. Hubral, 2001, Common- reflection-surface stack: Image and attributes: Geophysics, **66**, 97–109.

Neidell, N., and M. T. Taner, 1971, Semblance and other coherency measures for multichannel data: Geophysics, **36**, 482–497.

Salvador, L., and S. Savelli, 1982, Offset continuation for seismic stacking: Geophysical Prospecting, **30**, 829–849.

Santos, L., J. Scheicher, and M. Tygel, 1997, 2.5-D true-amplitude offset continuation: J. Seism. Expl., **6**, 103–116.

Schleicher, J., and C. Bagaini, 2004, Controlling amplitudes in 2.5D commom-shot migration to zero offset: Geophysics, **69**, 1299–1310.

Silva, E., 2005, Horizon velocity analisys using OCO rays: 9th International Congress, SBGf, Expanded Abstracts, 372:1–4.

Stolt, R., 2002, Seismic data mapping and reconstruction: Geophysics, **67**, 890–908.

Tygel, M., J. Scheicher, P. Hubral, and L. Santos, 1998, 2.5-D true-amplitude Kirchhoff migration to zero offset in laterally inhomogeneous media: Geophysics, **63**, 557–573.

Tygel, M., J. Schleicher, and P. Hubral, 1996, A unified approach to 3-D seismic reflection imaging - Part II:Theory: Geophysics, **61**, 759–775.